Operando DRIFTS study of the role of hydroxyls groups in trichloroethylene photo-oxidation over titanate and TiO_2 nanostructures

María D. Hernández-Alonso[a], Sergio García-Rodríguez[b], Silvia Suárez[a], Raquel Portela[a#], Benigno Sánchez[a] and Juan M. Coronado[c*]

a) Environmental Applications of Solar Energy, CIEMAT-PSA.

Avenida Complutense, 22, Bldg. 42. 28040 Madrid, Spain

b) Energía y Química Sostenible. Instituto de Catálisis y Petroleoquímica, Marie Curie 2, Cantoblanco, 28049 Madrid, Spain

c) Thermochemical Processes Unit. Instituto IMDEA Energía, Avenida Ramón de la Sagra, 3, Tecnomóstoles. 28933 Móstoles, Madrid, Spain

Present address: ICP-CSIC. Environmental Catalytic Processes Engineering, Marie Curie 2, Cantoblanco, 28049 Madrid, Spain

*Corresponding author

E-mail address: juanmanuel.coronado@imdea.org

Abstract

The aim of the present research was to gain further insight into the differences of the trichloroethylene photodegradation routes when using TiO_2 (Degussa P25) and protonated titanate nanotubes ($H_2Ti_3O_7$). These last materials present structural hydroxyls that, along with the surface OH groups present in both photocatalysts, could mediate in the mineralization of the pollutant. In order to obtain a realistic view, an operando Diffuse Infrared Fourier Transform Spectroscopy (DRIFTS) approach has been adopted for surface analysis during the photocatalytic oxidation. The study revealed that the trichloroethylene mineralization yield on the titanate nanotubes calcined at 300ºC was better than the one obtained with the benchmark photocatalyst Degussa P25. In particular, the synthesized nanotubes showed the selective removal of some specific hydroxyl groups, suggesting that their high density and, probably, the specific characteristics of their hydroxyl species can be responsible of the enhanced dechlorination photoactivity exhibited by these nanotubular structures.

Keywords:

Photocatalysis, Operando, DRIFTS, Trichloroethylene, Titanate, Nanotubes, TiO_2, Hydrothermal Synthesis

1. Introduction

Trichloroethylene (TCE) is a widespread pollutant in soils, aquifers and air streams [1] due to the fact that it has been extensively used as a solvent and degreasing agent in many industrial processes. Photocatalytic removal of this Volatile Organic Compound (VOC) has been frequently considered as an adequate remediation technique because TCE can be degraded with very high photonic efficiency [2,3]. However, in dry air streams, the formation of highly toxic $COCl_2$ (phosgene) takes place according to [2]:

$$C_2HCl_3 + \frac{3}{2}O_2 \rightarrow COCl_2 + HCl + CO_2 \quad (1)$$

In addition, dichloroacetyl chloride (DCAC), molecular chlorine and CO can be also detected in the outlet, depending on the reaction conditions [4]. The presence of water vapour could provide the hydrogen atoms required for the complete mineralization of TCE according to [5]:

$$C_2HCl_3 + \frac{3}{2}O_2 + H_2O \rightarrow 3HCl + 2CO_2 \quad (2)$$

Surface hydroxyl groups of TiO_2 have been reported to play a significant role in photocatalytic processes, acting as adsorption centres and electron donors in the formation of highly oxidant $OH^{\bullet}$ radicals [6]. Accordingly, it is expected that these surface species mediate in the mineralization of TCE. However, as molecular scale studies of photocatalysts are relatively scarce, the interactions of surface hydroxyls and organic molecules under illumination are still not fully understood. More recently, photocatalysts that present structural hydroxyls, such as protonated titanate nanotubes

with $H_2Ti_3O_7$ stoichiometry, have attracted a significant deal of interest [7,8] but little is known about the possible participation of these moieties on photoinduced reactions.

Photocatalytic degradation of TCE over TiO_2 and ZnO has been investigated by Fourier Transform Infrared (FTIR) spectroscopy [6,9,10]. These studies have identified dichloroacetate as the main adsorbed intermediate. Moreover, a different reactivity of pristine and used photocatalyst surfaces is suggested, in good agreement with the evolution of the photoactivity observed in independent reports [11]. Nevertheless, these studies were performed under idealized conditions, using reduced pressures of reagents and static atmospheres, while real applications take place in air streams at atmospheric pressure. Consequently, some relevant aspects of the process may have been overlooked in these pioneering spectroscopic analyses. In order to obtain a more realistic view, in the present study Diffuse Infrared Fourier Transform Spectroscopy (DRIFTS) with an *operando* approach has been adopted for surface analysis, which, as previous reports have confirmed, can provide valuable information about the mechanism of photocatalytic reactions [12]. In this work, the photoactivity for TCE degradation of titanate nanotubes, both as obtained after hydrothermal treatment and further calcined at 300ºC, was compared with the benchmark photocatalyst TiO_2 P25 in order to gain further insights on the possible differences on the TCE photodegradation routes.

2. Experimental Section

2.1 Synthesis of titanate nanotubes

The Ti-based nanotubular structures were obtained by hydrothermal treatment of commercial TiO_2 Degussa P25 (Evonik Degussa Corporation). For this purpose, 1 g of

P25 was hydrothermally treated at 130ºC in 70 mL of 10M NaOH in a Teflon-lined autoclave, for a period of 72 hours. The mixture was stirred for 30 min before and after the thermal treatment. In a second stage, the obtained powder was thoroughly washed in diluted HNO_3 and distilled H_2O. The powder was recovered from the solution by centrifugation and then dried at 100ºC overnight. A part of the synthesized material, labeled as TiNT-300ºC, was calcined for 3h at 300ºC.

2.2 Textural and structural characterization

BET surface area and average pore diameter values (Table 1) were estimated from N_2 adsorption isotherms, measured at 77 K in a Micromeritics 2100 automatic apparatus. Powder XRD patterns were recorded on an X'Pert Pro PANalytycal diffractometer using Ni-filtered Cu K_α radiation in the Bragg-Brentano geometry. Thermogravimetric analyses (TGA) were conducted under controlled atmosphere (75 ml/min air flow) in a Mettler Toledo TGA/SDTA851e thermobalance, from 25ºC to 800ºC with a heating rate of 5ºC/min.

A JEM-2100F 200 kV transmission electron microscope (JEOL Ltd.), equipped with an Oxford INCAx-Sight Energy Dispersive X-Ray Spectroscopy (EDS) detector (Oxford Instruments Ltd.), was used to study the crystallinity, chemical composition and morphology of the samples.

2.3 Photocatalytic Activity Measurements

The photocatalytic oxidation of gas-phase trichlotoethylene was studied in a continuous plug flow flat photoreactor described in detail elsewhere [5]. This reactor was constructed in stainless steel except for the top window of borosilicate glass with

low iron content. The photocatalyst samples were coated, after dispersion in 2-propanol, on a microscope slide that was located under the glass window. Irradiation was provided by two UVA fluorescent lamps (TL-8W/05, Philips) with a maximum emission at 365 nm wavelength and irradiance of 4.4 mW/cm^2. Flow rate, pressure, temperature, UV radiation and relative humidity were controlled by using electronic mass flow controllers and automated valves (Process Integral Development Eng&Tech S.L.). TCE concentration was fixed at 30 ppm, and total gas flow at 100 ml/min (residence time = 1.98 s). The gas-phase composition was continuously monitored using a FTIR Thermo-Nicolet 5700 spectrometer, provided with a temperature controlled multiple-reflection gas cell (optical path 2 m) maintained at 110 ºC. Selectivity to CO_2 was estimated according to the carbon balance (Eq. 1)

$$S_{CO_2} = \frac{CO_2}{2 \times (TCE_{inlet} - TCE_{outlet})} \times 100 \quad (1)$$

DRIFTS experiments were carried out in a Thermo Nicolet 5700 spectrometer equipped with a liquid N_2-cooled MCT detector and a Harrick three windows DRIFT high-temperature cell. Two of the catalytic chamber windows, made out of BaF_2, were used for IR transmission, and the third window was made out of quartz to allow the irradiation of the photocatalyst during the operando study of TCE photocatalytic oxidation. As irradiation source, two UVA Philips TL-8W/05 fluorescent lamps were used. The spectra were registered after accumulation of 64 scans at a resolution of 4 cm^{-1}. A continuous gas flow rate of 30 ml/min was applied, consisting of a mixture of TCE (ca. 65 ppm) and air. High purity dry gases, with residual water content lower than 5 ppm, were used for blending.

3. Results

3.1 Structural and morphological characterization of the studied photocatalysts

N_2 adsorption-desorption isotherms and pore size distributions, obtained from the adsorption branch of the isotherms, are displayed in Figure 1. Textural properties are summarized in Table 1. Degussa P25 shows an isotherm which has been usually described as type II, typical of non-porous or macroporous materials (pore size > 50 nm) [13], with a very low nitrogen uptake up to a relative pressure of ca. 0.8. The synthesized nanotubes exhibit type IV isotherms, associated to mesoporous materials, whose hysteresis loops can be described as intermediate of type H1 and H3. Type H1 is generally associated to mesoporous materials with uniform pores, while H3, characterized by the absence of a plateau at high relative pressures, is related to the presence of aggregates of laminar particles giving rise to slit-shaped pores [14]. Similar observations have been previously reported for titanate nanotubes [15,16]. Multimodal pore size distributions were obtained, with two small contributions at 2.3-2.6 nm and 3.9-4 nm, related to the inner diameter of the nanotubes, and a main feature centred at 25 nm which corresponds to the void space among nanotubes. No marked differences were observed in the textural properties of non-calcined TiNT and TiNT-300ºC; however, the slight decrease in the specific surface area, accompanied by a small increase in the total pore volume, seems to be associated with a larger contribution of small mesopores for calcined nanotubes.

Figure 2 shows the XRD patterns of the photocatalysts under study. The diffraction pattern of P25 shows the reflections due to anatase and rutile phases. The TiNT pattern shows a notably lower intensity and the identified peaks at 10.7, 24.9, 44.0, 48.9 and 62.2 º can be assigned to the protonated layered titanate. The reflection at

ca. 10.7º is attributed to the interlayer spacing in the nanotube wall. In the sample treated at 300ºC, no significant differences were observed with respect to the non-calcined material, but a slight shift to larger angles of the peak around 10º, which indicates a decrease in the spacing between the nanotube walls (d_{200}) [17], and a slight shift of the peaks at 24.9 and 48.9, indicative of the incipient transformation of the titanate structure into anatase.

The TEM analyses evidenced that, while P25 is constituted by prismatic particles with size ranging from 50 to 15 nm, hydrothermally treated samples show a nanotubular structure. Figure 3 reveals that this morphology is still maintained in the sample after calcination at 300ºC, which presents an entangled mass of nanotubes with very high aspect ratio. In fact, thermal treatment seems to promote the flawless scrolling of titanate sheets, as more uniform and well-formed nanotubes can be observed for the sample calcined at 300ºC.

3.2 Characterization of structural and adsorbed water on the photocatalysts

TGA curves (Figure 4) allowed estimating the total weight loss percentages of the samples with temperature in the 30-800ºC range, presented in Table 1. These weight losses can be mainly attributed to the elimination of physisorbed water, and crystallographic water. For Degussa P25 the weight loss was around 2%, while in the case of TiNT the total loss was ca. 14%. This higher percentage may be related not only to the higher surface area and thus, larger amount of physisorbed water, but also to the presence of crystallographic water and ion-exchangeable OH groups in the titanate structure ($H_2Ti_3O_7 \cdot xH_2O$) [17]. The titanate nanotubes (TiNT) underwent complete dehydration at 450-500ºC. Thus, this structural water will be partially removed during

the calcination treatment at 300ºC, and this removal could be associated to the shrinkage of the interlayer spacing d_{200} in the nanotubes walls, as deduced from XRD analyses.

DRIFT spectra of the fresh photocatalysts, acquired in air atmosphere (30 ml/min) after heating the samples at different temperatures (30ºC-500ºC), are presented in Figure 5. Although the intensity of the spectra of the titanate is remarkably higher, both Degussa P25 and nanotubes spectra exhibit a broad absorption region at 3600-2500 cm^{-1}, which correspond to adsorbed water molecules. These species show contributions of two different overlapping bands due to the vibrational modes of OH groups involved in H-bonds from multilayer H_2O molecular arrangements. The band at lower wavenumbers (ca. 3220 cm^{-1}) can be assigned to OH groups of tetrahedrally bonded water molecules, while the component at higher wavenumbers (ca. 3300 cm^{-1}) would correspond to hydroxyls from H_2O molecules with lower coordination [18].

In the 3775-3600 cm^{-1} region several narrow peaks are observed for P25 that are related to isolated hydroxyls or OH groups experiencing weaker intermolecular interactions. The presence of different components indicated the presence of more than one local structure for each type of hydroxyl species. At room temperature, three different bands can be identified in this area. The peaks at 3690 and 3630 cm^{-1} correspond to the stretching modes of free OH groups on Ti^{4+} of anatase, which interact with multilayer water [18], while the peak at 3648 cm^{-1} corresponds to Ti-OH on rutile [19]. At increasing temperatures, the intensity of the broad band at 3600-2500 cm^{-1} rapidly decreases due to water removal, while a peak appeared at 3415 cm^{-1}, which has been tentatively related to hydroxyl groups on rutile crystals [19]. As the temperature rose, two narrow peaks became more evident at 3715 and 3670 cm^{-1}. The first one can be ascribed to the stretching mode of terminal OH groups on Ti^{4+} centers, while the

second one can be assigned to bridging hydroxyls, whose proton is expected to be weakly bonded [18,20,21].

In the case of the titanate nanotubes, due to their considerably larger surface area, the intensity of the hydroxyl bands was almost one order of magnitude higher than in the case of TiO_2. Additional differences can be clearly observed when comparing both materials. Besides the expected absence of vibrational modes of Ti-OH on rutile, the predominance of one type of hydroxyl groups when increasing the temperature from 30 to 200ºC became evident. The band, at 3670 cm^{-1}, can be probably ascribed to bridging hydroxyls on the titanate nanotubes surface. Other prominent peak at 3725 cm^{-1}, which becomes evident at $T \geq 100$ºC, can be assigned to terminal hydroxyls. On one hand, the rate of water removal with temperature was significantly lower in TiNT than in TiO_2 P25, as estimated from the area under the curves. This is consistent with the fact that the crystallographic water from the protonated titanate nanotubes is less easily withdrawn than physisorbed or chemisorbed water. In the case of Degussa P25, adsorbed water was almost completely removed slightly above 200ºC.

3.2 Photocatalytic oxidation of trichloroethylene (TCE) – Gas phase analysis

Figure 6 displays the temporal evolution of the concentration of TCE and the noxious by-product $COCl_2$ as a function of the irradiation time. In all cases the efficiency for TCE removal increases very quickly during the initial period, then more gradually and finally remains basically constant. Under the selected operational conditions, TCE photo-oxidation over TiO_2 P25 led to complete elimination of this pollutant. Similarly, TCE conversion over TiNT-300ºC was close to 100%, while a considerably lower conversion (64%) was achieved over TiNT. This significant improvement in conversion obtained after calcination is remarkable considering the

similarities observed in the physicochemical characterization. The gradual evolution of the titanate structure into anatase with the increase in the calcination temperature is probably the cause of the boost in the photocatalytic activity of these nanotubular structures, although it entails a detriment in the selectivity to CO_2.

CO_2 and HCl were detected as main products from the oxidation of the volatile pollutant. However, as it has been previously observed, complete mineralization cannot be accomplished in the absence of water vapour in the gas stream and, consequently, products from side reactions, such as phosgene ($COCl_2$), CO and traces of dichloroacetyl chloride (DCAC), were also detected with the three types of photocatalyst [2-5]. As proposed by Jacoby et al., DCAC might be acting as intermediate to produce the different reaction products [22]. At the residence time used in this study (ca. 2 s) DCAC seems to have enough time to undergo further oxidation to produce $COCl_2$ and CO_x [23,24]. This is consistent with the fact that DCAC concentration in the outlet was rather small, while the intensity of $COCl_2$ and CO_2 signals was relatively high (Figure 7).

As it can be inferred from the data summarized in Table 2, titanate nanotubes inhibited the $COCl_2$ release, favouring the selectivity of CO_2. This fact was accompanied by a higher production of HCl and a lower detection of CO indicating that the mineralization process was enhanced in the case of the nanotubular photocatalysts. The calcination of TiNT sample at 300ºC led to an improvement in the photoactivity that resulted in a TCE conversion comparable to that of Degussa P25, but with a better selectivity to CO_2.

3.3 Operando DRIFTS study of the photocatalytic oxidation of TCE

Operando analysis of the photocatalysts surface during the photo-oxidation of TCE was conducted on an attempt to explain the different performance observed for the titanate nanotubes with respect to TiO_2 nanocrystals.

Figure 8 presents the time-resolved DRIFT spectra in the 1750-1150 cm^{-1} region of trichloroethylene photo-oxidation on the different photocatalysts tested. In spite of the extensive band overlapping, which renders difficult the unequivocal identification, the presence of some surface complexes can be inferred from previously proposed mechanisms and assignments. Thus, bands at ca. 1598, 1410 and 1225-1229 cm^{-1} can be attributed to different adsorbed dichloroacetate species, formed from the hydrolysis of DCAC. The bands at around 1575, 1375 and 1360 cm^{-1} could be related to the presence of adsorbed formate [9,10,25,26]**¡Error! Marcador no definido.**. The weak band at 1660 cm^{-1} observed in Degussa P25 spectrum could be tentatively attributed to the presence of adsorbed phosgene as bidentate complexes, which would be also contributing to the band at 1229 cm^{-1} [10,27**¡Error! Marcador no definido.**]. This last band can be related to vibrations of the -$CHCl_2$ group, and it is worth noting that it is more intense in the case of P25, indicating that a larger concentration of halogenated organic intermediates builds up on the surface of this photocatalysts. In contrast, as the characteristic band of carbonates at about 1000 cm^{-1} is missing in all the spectra, it seems that these species are not formed in significant amounts. Yet, a more detailed assignment is required in order to further establish the differences between samples, which are remarkable, as it can be appreciated in Figure 8. Deconvolution of the spectra for TiO_2 and calcined nanotubes, shown in Figure 9, reveals that at least three different carboxylate species, with different coordination symmetry (e.g. bridged dichloroacetate, bidentate formate…) are present on the surface of these samples. In the case of the untreated nanotubes, the spectrum is dominated by strong bands at 1558 and 1542 cm^{-1},

which can be attributed to the asymmetric vibration of additional carboxylate complexes, with either different topology or coordinated to some specific sites of the surface of these nanostructures. According to this assignment, the main difference between TiO_2 and nanotubes seems to be the larger proportion of formate species for the two titanate samples, which is more prominent for the case of the non-calcined sample TiNT. A summary of all these assignments is outlined in Table 3. On the other hand, the intensity of the bands in this region is notably higher for the nanotubes calcined at 300ºC than for the other samples, which present much more similar absorbance. This fact is probably due to the combination of large surface area and relatively high photoactivity of these thermally treated nanotubes, which promote the building up of reaction products.

Figure 10 displays the time-resolved DRIFT spectra in the 4000-2500 cm^{-1} range of operando photocatalysts. Despite the fact that all the different types of isolated hydroxyls, terminal Ti-OH (basic) and bridging OH (acidic), were involved in TCE adsorption (spectra not shown), during the photocatalytic reaction terminal Ti-OH remain unchanged. In contrast, bridging OH groups were consumed during TCE photodegradation for the three catalysts, as evidenced by the decreasing peak at 3690 cm^{-1}. However, significant differences can be observed between the behaviour of the commercial photocatalyst Degussa P25 and the home-synthesized titanate nanotubes. Under irradiation Degussa P25 experienced the perturbation of different types of hydroxyl groups, as pointed out by the negative peaks at around 3690, 3685, 3670 and 3630 cm^{-1}. This intensity loss is associated with an adjacent positive feature which can be related to the hydrogen bonding with TCE or the products of its degradation [9]. On the other hand, the spectra of titanate nanotubes were dominated by a strong negative band centered at ca. 3682 cm^{-1}, accompanied by the loss of coordinated water

molecules, as shown by the broad negative band centred at about 3200 cm^{-1}. These results indicate a remarkable specificity of the hydroxyls involved in the photocatalytic reactions on nanotubes. In addition, it is worth mentioning that in contrast to the case of carboxylates, the intensity of these bands is relatively similar for all the samples, although the larger hydroxyl losses correspond to the nanotubes. The evolution profiles of hydroxyl groups on the samples surfaces during the photocatalytic reaction, extracted from the peak height at ca. 3690-3682 cm^{-1} of the spectra in Fig. 9, are shown in Fig. 11. An opposite tendency can be observed for the build-up carboxylates on the surface, as estimated from the intensity of the band at ca. 1580 cm^{-1}. These facts suggest that the following reaction between photogenerated DCAC and specific bridging hydroxyls is taking place according to:

$$CCl_2\text{-}COCl + \text{-}Ti^{4+}\text{-}OH^{-}\text{-}Ti^{4+} \rightarrow (CCl_2\text{-}COO^{-})(Ti^{4+})_2 + HCl \quad (3)$$

Therefore, these centres seem to participate in dechlorination reactions which are crucial for TCE mineralization. Nevertheless, while hydroxyls decay tends to approach an asymptotic value for longer irradiation periods, carboxylates show a more gradual, almost linear growth. This fact suggests that other species can be also contributing to the more rapid consumption of these active hydroxyls centres. However, as photoactivity is very stable for all catalysts, it seems that these species are in a dynamic equilibrium, with significant number of centres still available for adsorption and surface reaction. According to the obtained reactivity data, the degradation of DCAC, adsorbed as dichloroacetate, can be considering the rate determining step [4], while the detection of adsorbed $COCl_2$ on P25 may be related to the higher difficulty in degrading this by-product on TiO_2 as compared to titanate nanotubes.

Despite the complexity of the surface composition of these nanostructured catalysts under operando conditions, some similarities in the behaviour of the three

photocatalysts can be extracted from these results. Leaving apart changes in coordination and relatively small variations in intensity, surface complexes are similar for the three samples, suggesting that photodegradation occurs in a similar way in all cases. Dichlorocetate and other carboxylates are the predominant surface species, and progressively accumulate on the photocatalytic surface. Simultaneously, hydroxyl groups are consumed, and this fact can be related to the interaction of DCAC and other intermediates with these centres. Previous studies have revealed the relevance of adsorbed water and hydroxyl to promote TCE photocatalytic mineralization [5]. However, this study shows that highly specific reactivity of the hydroxyls can be crucial for the hydrolysis of phosgene on nanotubes, although further studies are required to confirm this point.

5. Conclusions

The present study indicates that after thermal treatment the titanate nanotubes retain most of the physicochemical characteristics of the hydrothermally prepared sample, such as large surface area and high water content, but the photocatalytic activity is greatly enhanced. In particular, titanate nanotubes calcined at 300ºC present better TCE mineralization yield than the benchmark photocatalysts TiO_2 P25.

The present operando DRIFTS study has revealed some relevant differences between the studied catalysts, although the TCE photo-oxidation mechanism is similar in general terms. In particular, the nanotubes suffer the selective removal of some specific hydroxyl groups, very likely due to the progressive accumulation on the photocatalyst surface of carboxylate complexes (mainly dichloroacetate and formate) and/or chloride. The obtained results suggest that the high density, and probably the

specific characteristics of the hydroxyls species, which seem to favor dechlorination processes, are responsible for the enhanced selectivity to CO_2 of the nanotubes.

Acknowledgments

Financial support from the Spanish Ministry of Science and Innovation (MICINN, MAT2008-01094/MAT) is greatly appreciated. M.D.H. and S.S also thank MICINN for the award of a postdoctoral contract.

References

(1) C. Fan, G-S Wang, Y. C. Chen, C. H. Kod, Sci. Total Environ. 407 (2009) 2165.

(2) S. Yamazaki-Nishida, S. Cervera-March, K.J. Nagano, M.A. Anderson, K. Hori, J. Phys. Chem. 99 (1995) 15814.

(3) J. M. Coronado, B. Sanchez, R. Portela, S. Suarez, J. Solar Energy Eng. 113 (2008) 0110161.

(4) Jacoby, W.A.; Nimlos, M.R.; Blake, D.M.; Noble, R.D.; Koval, C.A. Environ. Sci. Technol. 28 (1994) 1661.

(5) Suárez, S.; Coronado, J.M.; Portela, R.; Martín, J.C.; Yates, M.; Ávila, P.; Sánchez, B. Environ. Sci. Technol. 42 (2008) 5892.

(6) K.L. Yeung, S.T. Yau, A. J. Maira, J. M. Coronado, J. Soria y P. L. Yue, J. Catal. 219 (2003) 107.

(7) B.C. Viana, O.P. Ferreira, A.G. Souza, C.M. Rodrigues, S.G. Moraes, J. Mendes, O.L. Alves, J. Phys. Chem. C 113 (2009) 20234.

(8) H.Y. Zhu, Y. Lan, X.P. Gao, S.P. Ringer, Z.F. Zheng, D.Y. Song, J.C. Zhao, J. Amer. Chem. Soc. 127 (2005) 6730.

(9) M. D. Driessen, A. L. Goodman, T. M. Miller, G. A. Zaharias, and V. H. Grassian, J. Phys. Chem. B 102 (1998) 549.

(10) S.-K. Joung, T. Amemiya, M. Murabayashi, K. Itoh, J. Photochem. Photobio. A 184 (2006) 273.

(11) B. Sanchez, J. M. Coronado, R. Candal, R. Portela, I. Tejedor, M. A. Anderson,D. Tompkins, T. Lee, Appl. Catal. B 66 (2006) 294.

(12) M. D. Hernández-Alonso, I. Tejedor-Tejedor, J. M. Coronado, M. A. Anderson, J. Soria, Catal. Today 143(2009) 364.

(13) F. Rouquerol, J. Rouquerol, K. Sing, "Adsorption by Powders and Porous Solids: Principles, Methodology and Applications", Academic Press, Londres (1999).

(14) S. J. Gregg, K. S. W. Sing, “Adsorption, Surface Area and Porosity”, Academic Press, Londres (1982).

(15) Bavykin, D.V.; Parmon, V.N.; Lapkin, A.A.; Walsh, F.C. J. Mater. Chem. 14 (2004) 3370.

(16) Morgado, E.; de Abreu, M.A.S.; Moure, G.T.; Marinkovic, B.A.; Jardim, P.M.; Araujo, A.S. Chem. Mater. 19 (2007) 665.

(17) D.V. Bavykin, M. Carravetta, A.N. Kulak, F.C. Walsh, Chem. Mater. 22 (2010) 2458.

(18) J. Soria, J. Sanz, I. Sobrados, J. M. Coronado, A. J. Maira, M. D. Hernández-Alonso, F. Fresno, J. Phys. Chem. C 111 (2007) 10590.

(19) C. Morterra, J. Chem. Soc. Faraday Trans. 84 (1998) 1617.

(20) P. A. Connor, K. D. Dobson, A. J. McQuillan, Langmuir 15 (1999) 2402.

(21) K. S. Finnie, D. J. Cassidy, J. R. Bartlett, J. L. Woolfrey, Langmuir 17 (2001) 816.

(22) W.A. Jacoby, D.M. Blake, R.D. Noble, C.A. Koval, J. Catal. 157 (1995) 87.

(23) Fan, J.; Yates, J. T., Jr. J. Am. Chem. Soc. 118 (1996) 4686.

(24) T.L.R. Heder, S. Suárez, J.M: Coronado, R. Portela, P. Ávila, B. Sánchez, Catal. Today 143 (2009) 302.

(25) M.D. Driessen, T.M. Millar, V.H. Grassian, J. Mol. Catal. A-Chem. 131 (1998) 149.

(26) J.-S. Kim, K. Itoh, M. Murabayashi, Chemosphere 36 (1998) 483.

(27) S.-K. Joung, T. Amemiya, M. Murabayashi, R. Cai, K. Itoh, Surf. Sci. 598 (2005) 174.

Table 1.

Textural properties and total weight loss percentages, estimated from TGA analysis (30-800ºC), of the photocatalysts.

Sample	Post-synthesis thermal treatment	S_{BET} (m^2/g)	Total pore volume, cm^3/g	Weight loss , %
Degussa P25	-	48	0.29	2
TiNT	100ºC, overnight	419	1.37	14
TiNT-300ºC	300ºC, 3h	356	1.45	10

Table 2.

Gas-phase TCE photocatalytic degradation results at the steady state. Intensity is measured as the integrated area of the corresponding selected FTIR band.

Muestra	I_{HCl} (a.u.)	I_{CO} (a.u.)	I_{DCAC} (a.u.)	CO_2 (ppm)	$COCl_2$ (ppm)	TCE conversion (%)	Selectivity to CO_2 (%)
Degussa P25	0.017	0.230	0.003	36	26	100	60
TiNT	0.088	0.175	0.004	24	12	64	64
TiNT-300ºC	0.084	0.171	0.008	38	20	96	66

Table 3.

Assignment of the IR bands of surface species formed during the photocatalytic degradation of TCE.

Surface species	Vibration mode	Frequency (cm^{-1})*	
		Observed	**Literature**
Dichloroacetate – monodentate	ν (C=O)	1741	1731
Phosgene	ν_{as} (COO)	1649, 1662	1620-1670
	ν_{s} (COO)	-	1238
Dichloroacetate – bidentate	ν_{as} (COO)	1599, 1601	1611
	ν_{s} (COO)	1392	1393
	δ (CH-Cl_2)	1225, 1228	1220-1228
Dichloroacetate – bridged bidentate	ν_{as} (COO)	1587	1581-1591
	ν_{s} (COO)	1410, 1412	1418
	δ (CH-Cl_2)	1225, 1228	1220-1228
Formate - bidentate	ν_{as} (COO)	1573-1577	1575
	ν_{s} (COO)	1379	1362
	δ (C-H)	1359, 1361	1379

* Refs. [9,10,25-27].

Figure 1.

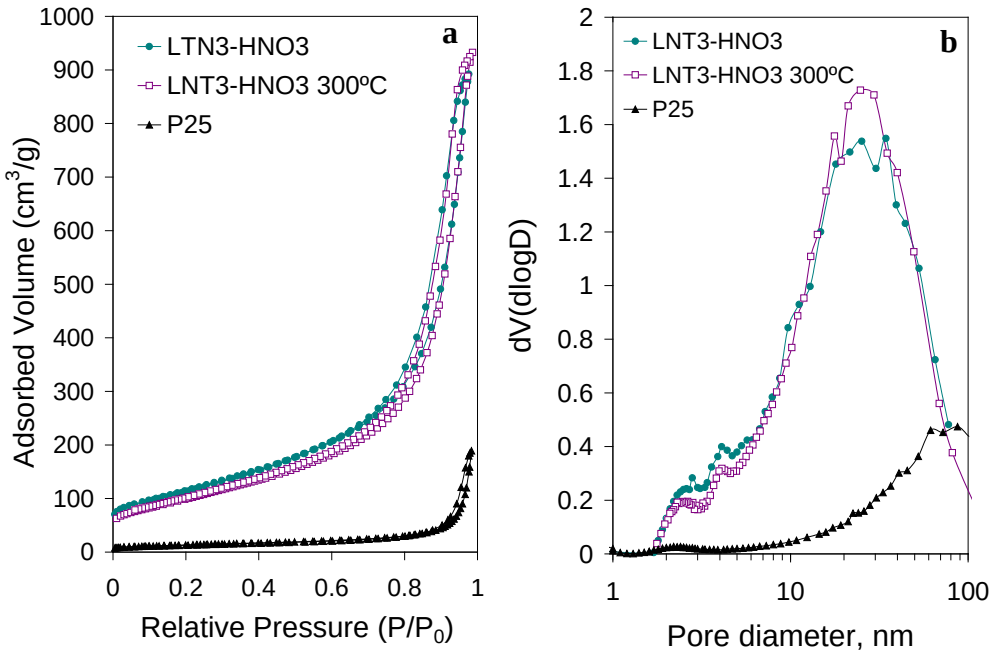

Fig. 1 – (a) N_2 adsorption-desorption isotherms and (b) pore size distribution of Degussa P25 and the synthesized photocatalysts.

Figure 2

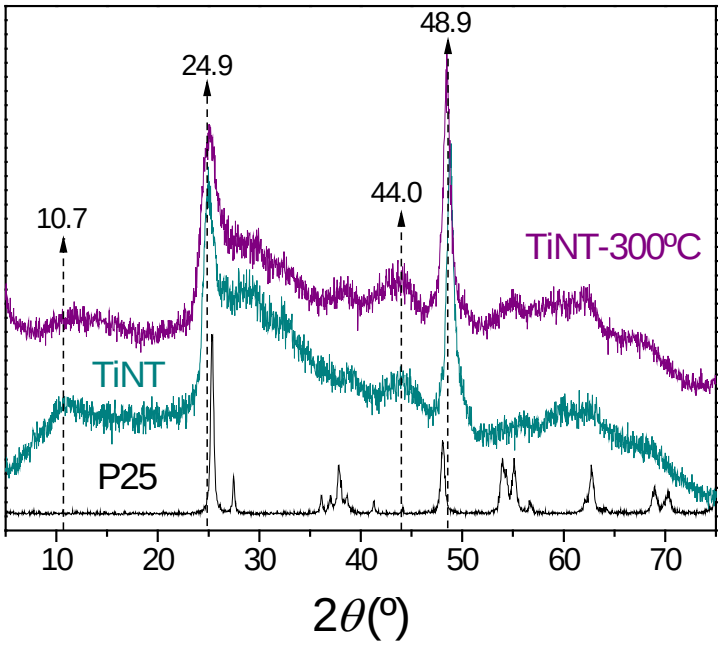

Fig. 2 – XRD patterns of the titanate nanotubes. Degussa P25, consisting on a mixture of anatase and rutile, is shown as reference.

Figure 3

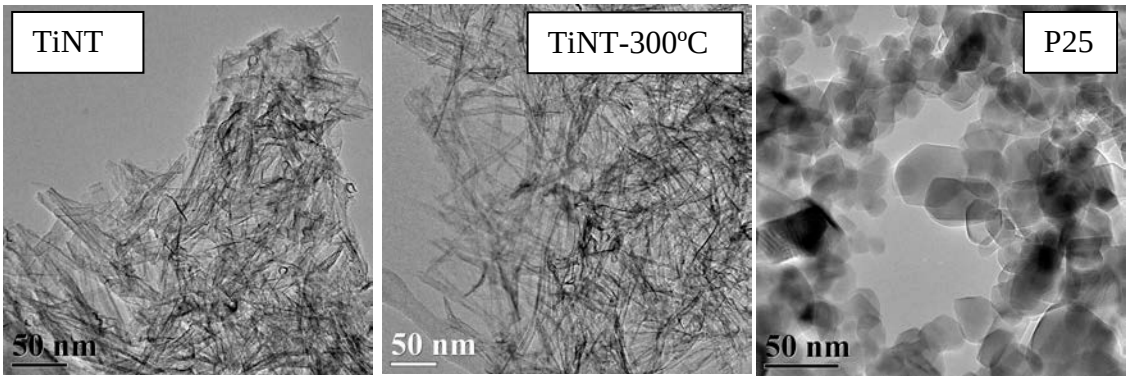

Fig. 3 – TEM micrographs of TiNT, TiNT-300ºC and Degussa P25, used as precursor in the synthesis and also as the reference photocatalyst.

Figure 4

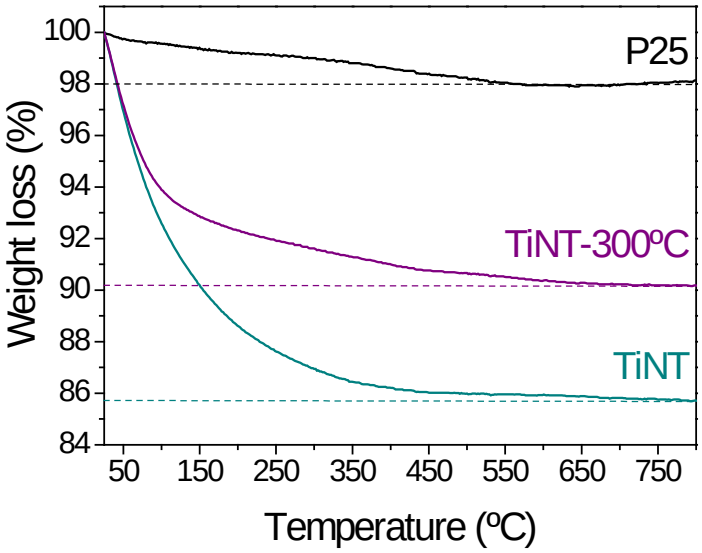

Fig. 4 – TGA curves registered at a scan rate of 5 ºC/min.

Figure 5

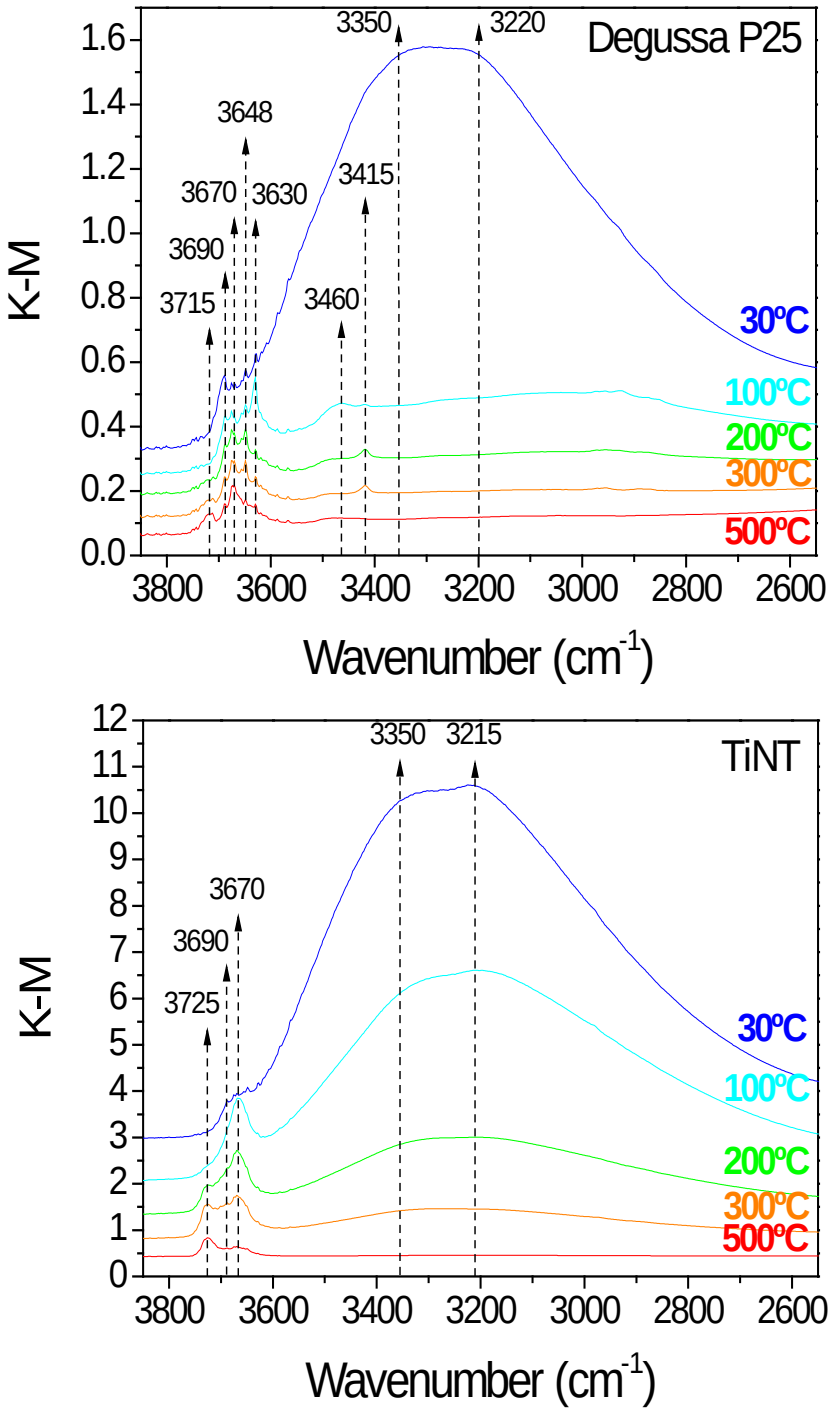

Fig. 5 - Detail of the fresh photocatalysts DRIFT spectra, registered in air atmosphere (30 ml/min), after heating the samples at different temperatures: 30, 100, 200, 300 and 500ºC.

Figure 6

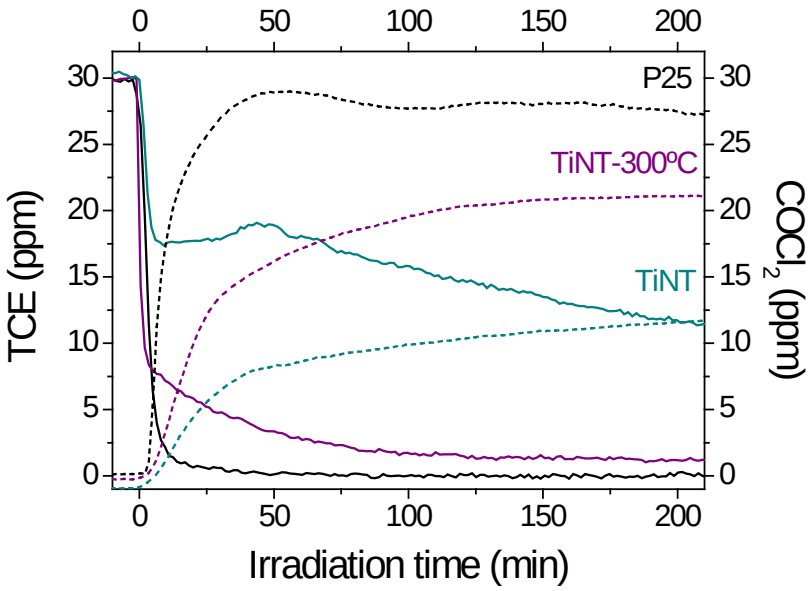

Fig. 6 - Evolution of TCE (solid lines) and $COCl_2$ concentration (dash lines) with irradiation time.

Figure 7

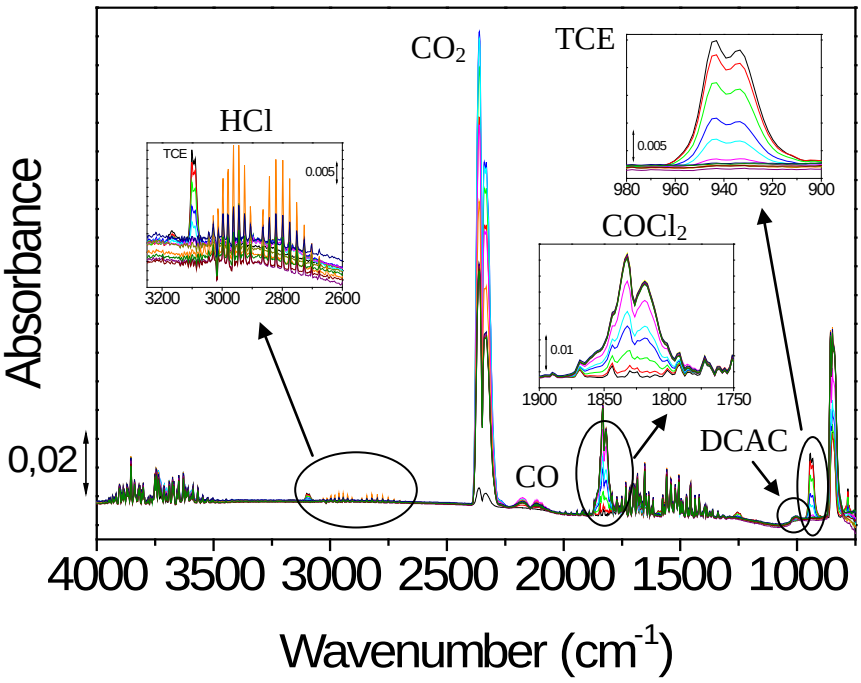

Fig. 7 - FTIR spectra of the gas phase during the photocatalytic degradation of TCE on Degussa P25. The bands selected to follow the evolution of each compound have been marked. The contributions from water and DCAC were subtracted from the $COCl_2$ signal while the contribution from $COCl_2$ was subtracted from the CO_2 feature.

Figure 8

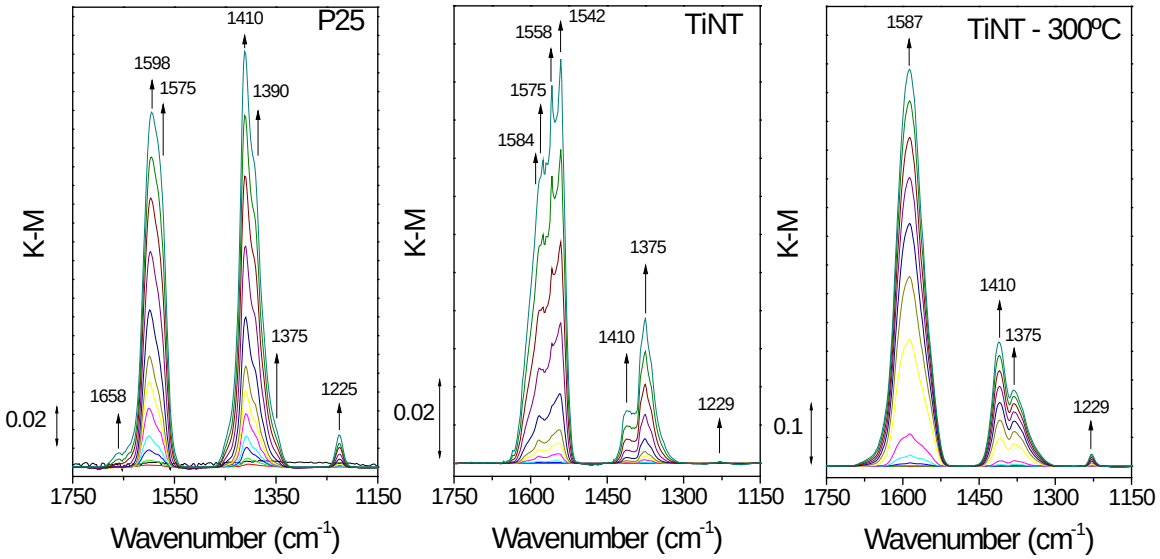

Fig. 8 - Time-resolved DRIFT spectra (1750-1150 cm^{-1} interval) of trichloroethylene photo-oxidation on the different photocatalysts tested at 0.5, 1, 2, 5, 10, 20, 30, 40, 60, 90, 120, 150 and 180 min of irradiation. The spectrum of each catalyst at the adsorption equilibrium was used as background. Arrows pointing up indicate increasing peaks.

Figure 9

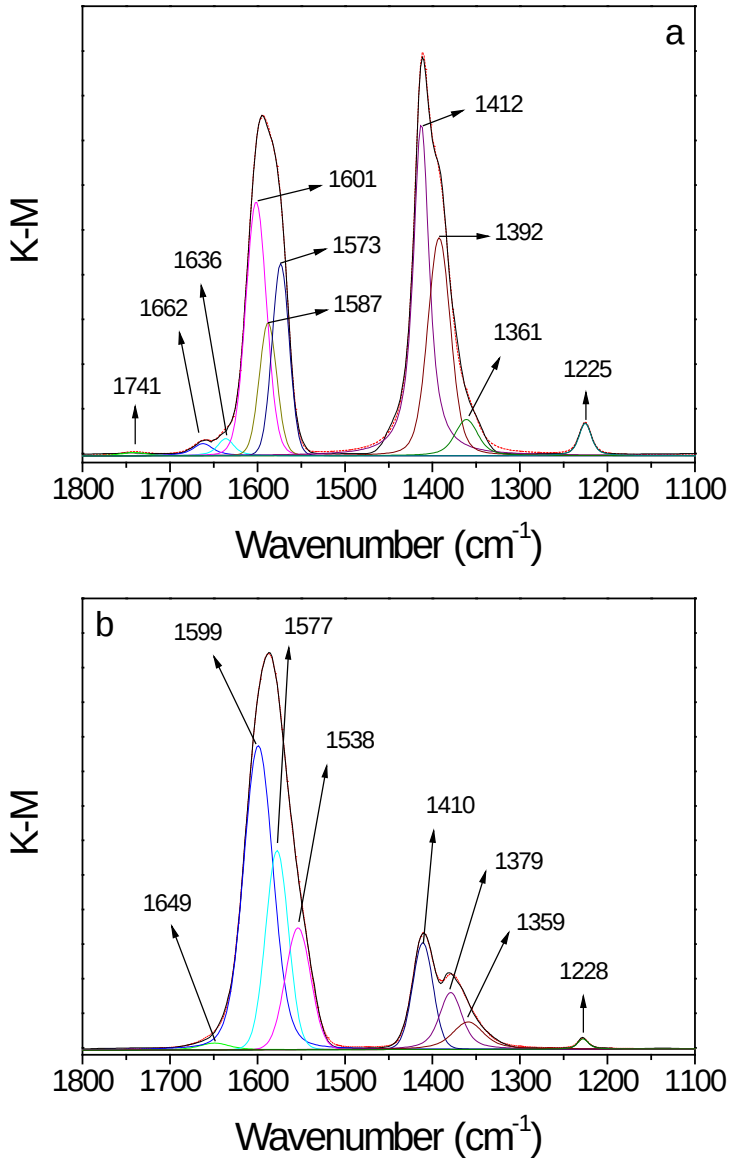

Fig. 9 – Results of the deconvolution of the DRIFT spectra obtained during the photocatalytic degradation of TCE, at 180 min of irradiation, on (a) Degussa P25; and (b) TiNT-300ºC.

Figure 10

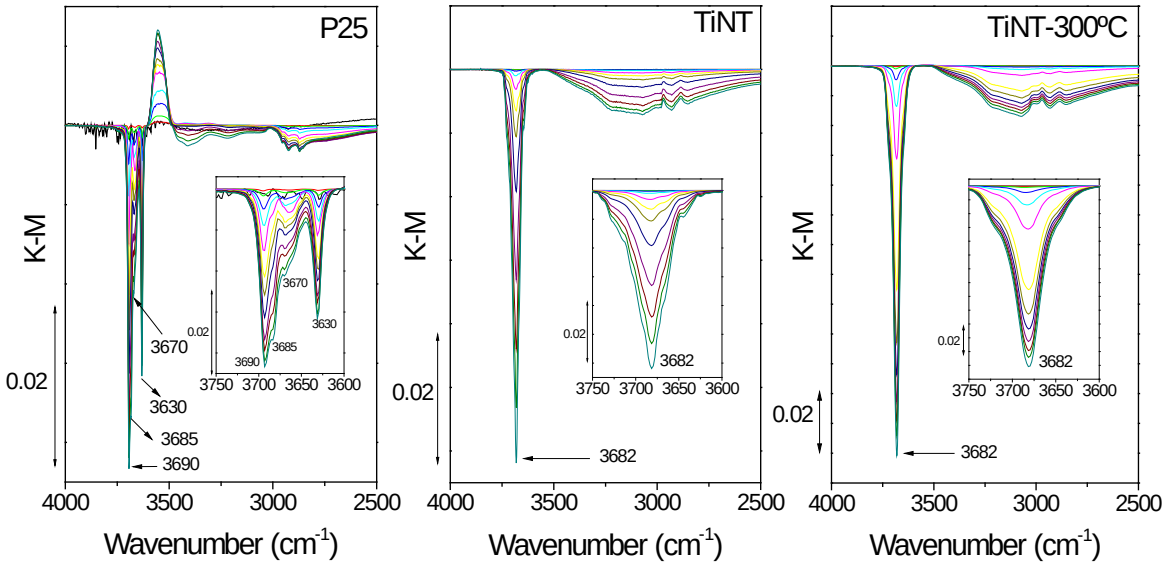

Fig. 10 - Time-resolved DRIFT spectra (4000-2500 cm^{-1} interval) of trichloroethylene photo-oxidation on the different photocatalysts tested at 0.5, 1, 2, 5, 10, 20, 30, 40, 60, 90, 120, 150 and 180 min of irradiation. The spectrum of each catalyst at the adsorption equilibrium was used as background.

Figure 11

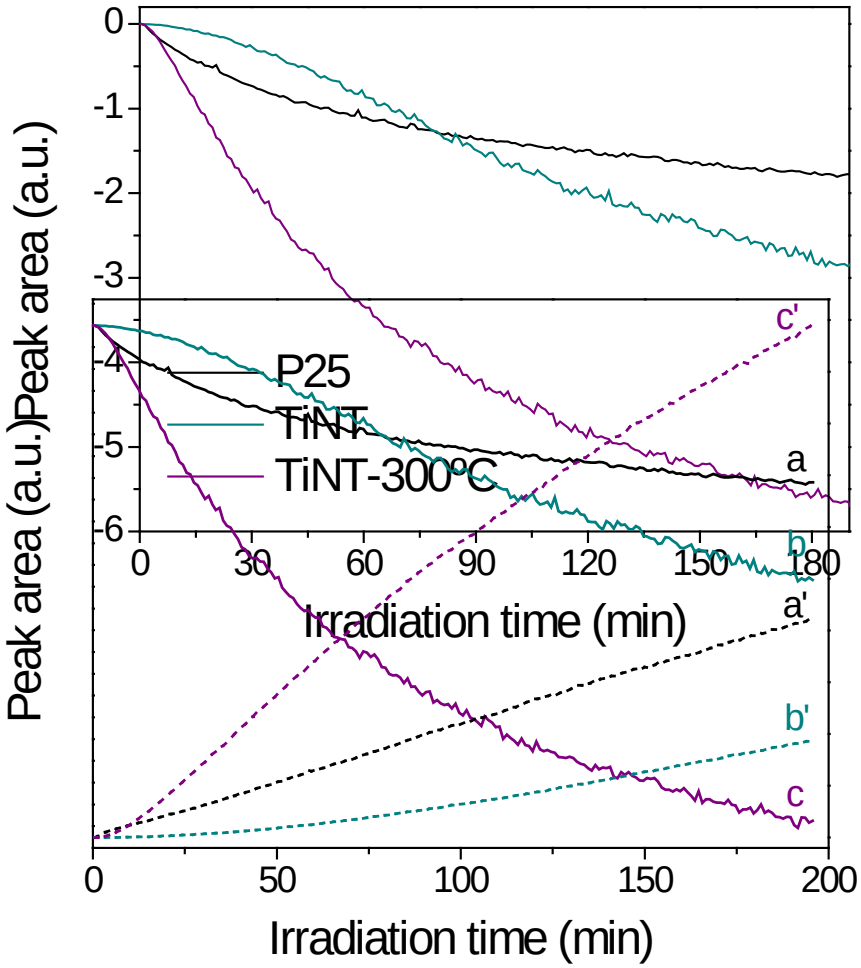

Fig. 11 - Evolution of the surface hydroxyl groups (peak area 3780-3600 cm^{-1}) and the carboxilate species (peak area 1750-1500 cm^{-1}) on (a, a') Degussa P25; (b,b') TiNT; (c,c') TiNT-300ºC